THE JOURNAL OF PHYSICAL CHEMISTRY C

Article

pubs.acs.org/JPCC

Impact of the Anchoring Ligand on Electron Injection and Recombination Dynamics at the Interface of Novel Asymmetric Push–Pull Zinc Phthalocyanines and TiO_2

Divya Sharma,[†] Gerwin Steen,[†] Jeroen P. Korterik,[†] Miguel García-Iglesias,[‡] Purificacion Vázquez,[‡] Tomás Torres,[‡,§] Jennifer L. Herek,[†] and Annemarie Huijser*[,†]

[†]Optical Sciences group, MESA+ Institute for Nanotechnology, University of Twente, P.O. Box 217, 7500 AE, Enschede, The Netherlands

[‡]Departamento de Química Orgánica, Universidad Autónoma de Madrid, 28049 Madrid, Spain

[§]IMDEA-Nanociencia, Campus de Cantoblanco, c/Faraday 9, 28049 Madrid, Spain

Supporting Information

ABSTRACT: Phthalocyanines are promising photosensitizers for dye-sensitized solar cells (DSSCs). A parameter that has been problematic for a long time involves electron injection (EI) into the TiO_2. The development of push–pull phthalocyanines shows great potential to improve the ratio of EI to back electron transfer (BET). We have studied the impact of the anchoring ligand on EI and BET using transient absorption. The best performing derivative, which has a dicarboxylic acid anchoring ligand (TT15, DSSC efficiency of 3.96%), shows the fastest EI. The EI process occurs via an ultrafast component (~700 fs for all derivatives) and a slower component (5.8 ps for TT15). The ps component is considerably slower for the other derivatives studied. Also BET depends on the anchoring ligand and is the slowest for TT15. This knowledge is essential for the optimization of the EI/BET ratio and the efficiency of a phthalocyanine-based DSSC.

INTRODUCTION

The dye-sensitized solar cell (DSSC) is a low-cost alternative to conventional solid-state photovoltaic devices.[1] The heart of a DSSC involves the interface between a semiconductor nanoparticle (usually TiO_2) and a photosensitizer molecule. Excitation of the photosensitizer should lead to efficient electron injection (EI) into the semiconductor; recombination or back electron transfer (BET) has to be avoided to allow electrons to diffuse away from the interface. Among the most successful photosensitizers are polypyridylruthenium complexes, with efficiencies up to 10–11%.[2,3] In the region with strong absorption, incident photons are converted into charges with close to unity efficiency, indicating a high EI/BET ratio. Utilization of the red part of the visible spectrum where the solar flux is maximum is however problematic due to lack of absorption in this region.

Phthalocyanines are well-known for their intense absorption in the red/near-IR region of the solar spectrum and excellent photochemical stability. DSSC devices based on phthalocyanines, however, have shown efficiencies below 1% for a long time.[4,5] This is likely caused by a low EI/BET ratio. Recently, significantly higher efficiencies up to about 6% have been realized.[6−14] An important tool in the development toward higher efficiencies involves the prevention of aggregation and the introduction of directionality in the electron transfer process. Only the chemical functionality anchored onto the TiO_2 should attract the electron, while functionalities not attached to the TiO_2 should be both electron-pushing and bulky enough to prevent aggregation.

An important aspect to address is the ideal chemical structure of the anchoring group. It should attach the phthalocyanine molecule onto the semiconductor. Carboxylic acid functionalities are known to bind to metal oxide surfaces and therefore often applied as anchoring side group.[15,16] According to the Marcus theory,[17] the electronic coupling between electron donor and acceptor is an important parameter determining the electron transfer rate. The mutual orientation of the phthalocyanine core and the TiO_2 acceptor is thus likely to affect both the EI and BET dynamics. It is, however, unclear whether adapting the distance between phthalocyanine and TiO_2 and the mutual orientation of electron donor and acceptor affects both processes in a similar manner and keeps the EI/BET ratio constant or allows tuning the dynamics in favor of the EI process.

Typical EI times range from fs till ps; generally, both a fs and a ps component are observed.[18−22] These two time constants are usually ascribed to a two-state relaxation model, with the fast component resulting from EI from the nonthermalized state and the slower component originating from the relaxed excited state. The discrepancy in time scales is attributed to a variation in density of states in the TiO_2 with energy.[18,20] An alternative explanation for the occurrence of two time constants involves the combination of EI directly from the molecule into the TiO_2, occurring on a fs time scale, and intermolecular energy transfer on a ps time scale.[19,22] BET processes could

Received: October 10, 2013
Published: November 12, 2013

occur in a wide time window ranging from the sub-ps to the μs-ms domain. Fast BET has been ascribed to electrons localized on Ti atoms with a strong electronic coupling with the anchored photosensitizer radical cation, while delocalized electrons contribute to slower BET processes.[23−25]

Several groups have investigated the effect of electronic coupling between photosensitizer and TiO_2 on EI and BET dynamics by adapting the anchoring group and the linker. A carboxylic acid anchoring group was found to give a higher EI/BET ratio than an alkyl group.[26,27] Inserting $-CH_2$-linking groups between a Re polypyridyl complex and TiO_2 was observed to decrease the EI rate.[28] Diau and co-workers studied the impact of introducing oligo(phenylethynyl) linkers between a zinc porphyrin and TiO_2 on the ultrafast dynamics to understand the observed impact on the DSSC efficiency. The EI rate appeared to be independent of the linker,[29] while zinc porphyrins with a longer linker showed faster BET.[30] A similar trend was observed for triphenylamine-based photosensitizers.[31]

Only a few papers report on the ultrafast interface dynamics of symmetrical zinc phthalocyanines and TiO_2. The EI process from a zinc phthalocyanine derivative equipped with four tyrosine side groups into TiO_2 nanoparticles was found to occur within 500 fs. The BET process occurs at time scales ranging from tens of ps to ns.[5] The EI process from zinc phthalocyanine into a flat TiO_2 (110) layer was observed to occur on a time scale ≤300 fs.[32] All these symmetrical zinc phthalocyanines perform poor in a DSSC. The ultrafast interface dynamics of asymmetrical zinc phthalocyanines showing significantly higher DSSC efficiencies have not been reported so far.

We have recently synthesized a series of asymmetrical zinc phthalocyanines with different anchoring ligands (Scheme 1).[33] All derivatives are equipped with three *tert*-butyl bulky side groups to suppress aggregation. The fourth ligand has been tuned systematically from a carboxylic acid only (TT1) to more bulky anchoring groups with a spacer in between the phthalocyanine core and the carboxylic acid group (TT6, TT7, and TT15). The TT6 derivative has a conjugated bridge in between the molecular core and carboxylic acid group and was observed to perform slightly inferior to the standard TT1 dye (TT6: 3.28% vs TT1: 3.56%). TT7 is a derivative of TT6 and equipped with an electronegative CN group attached to the conjugated bridge to promote directionality of the electron transfer. Surprisingly, TT7 was observed to give an efficiency of 2.55% only. It is not clear whether this is due to unfavorable EI, BET, or both. TT15 is also derived from TT6, but has instead a second anchoring carboxylic acid group attached to the conjugated bridge. This derivative gives a DSSC efficiency as high as 3.96%.[33] More details regarding the DSSC characteristics are provided in Figure 1 and Table 1 of the Supporting Information. In current work we study the EI and BET dynamics of all four derivatives attached to TiO_2 nanoparticles using ultrafast transient absorption spectroscopy. We will address whether the difference in DSSC efficiency observed (see Scheme 1) is due to a change in the EI and/or BET dynamics.

Scheme 1. Molecular Structures of the Zinc Phthalocyanines TT1, TT6, TT7, and TT15, and the Efficiencies of DSSCs Based on These Derivatives[33]

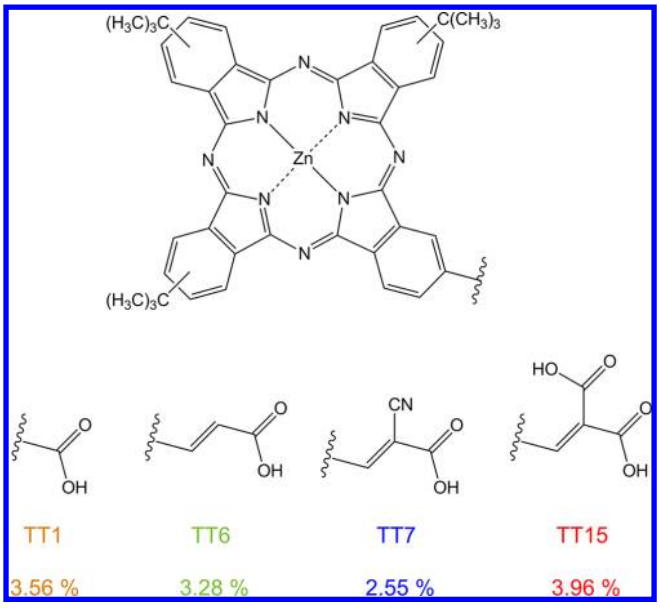

EXPERIMENTAL SECTION

Sample Preparation and Steady-State Characterization. Colloidal TiO_2 paste (Ti-nanoxide HT/SC) was purchased from Solaronix SA. The nanoparticle diameter is specified to be 8−10 nm. A nanoporous TiO_2 film was prepared by spreading the paste onto a microscope glass slide, followed by taking off the excess by using a glass rod. After removing the tape used as a spacer and drying in air for 24 h, the sample was annealed in air at 450 °C for 30 min to obtain a transparent nanoporous TiO_2 film. The film thickness was measured using a Dektak profilometer to be 1.5 μm.

The synthesis of the zinc phthalocyanine derivatives TT1, TT6, TT7, and TT15 was described in refs 10 and 33. A solution of 0.5×10^{-4} M of the zinc phthalocyanine derivative and 20 mM chenodeoxycholic acid (Sigma Aldrich) in ethanol (Uvasol, ethanol for spectroscopy) was used for sensitization of the TiO_2. After annealing at 450 °C and cooling down to 80 °C, the TiO_2 slide was immersed into the dye solution for 4 h and rinsed quickly several times with ethanol after taking the sample from the dye solution. All samples were prepared just prior to the experiment. Transient absorption measurements were performed both in the absence and in the presence of acetonitrile (mimicking the electrolyte) covering the dye-sensitized film. The latter was realized by placing a spacer frame with a thickness of about 0.1 mm on top of the sample, filling the space with acetonitrile, followed by covering the sample with a thin microscope glass slide. Since no significant impact of the presence of acetonitrile on the dynamics was observed (see Supporting Information, Figures 2 and 3) and the acetonitrile was gradually evaporated during the recording of several data sets, the systematic comparison of TT1, TT6, TT7, and TT15 was performed in air instead. The sample was mounted on an automated mechanical translational stage to avoid any impact of photodegradation on the ultrafast dynamics. Significant chemical degradation due to illumination was excluded on the basis of similar optical absorption spectra before and after the experiments.

Femtosecond Transient Absorption. The femtosecond transient absorption setup used was described in ref 38. Briefly, part of the output of an amplified Ti:Sapphire laser system (Clark CPA-2001) was sent into a noncollinear optical parametric amplifier (NOPA) and compressed afterward

dx.doi.org/10.1021/jp410080a | J. Phys. Chem. C 2013, 117, 25397−25404

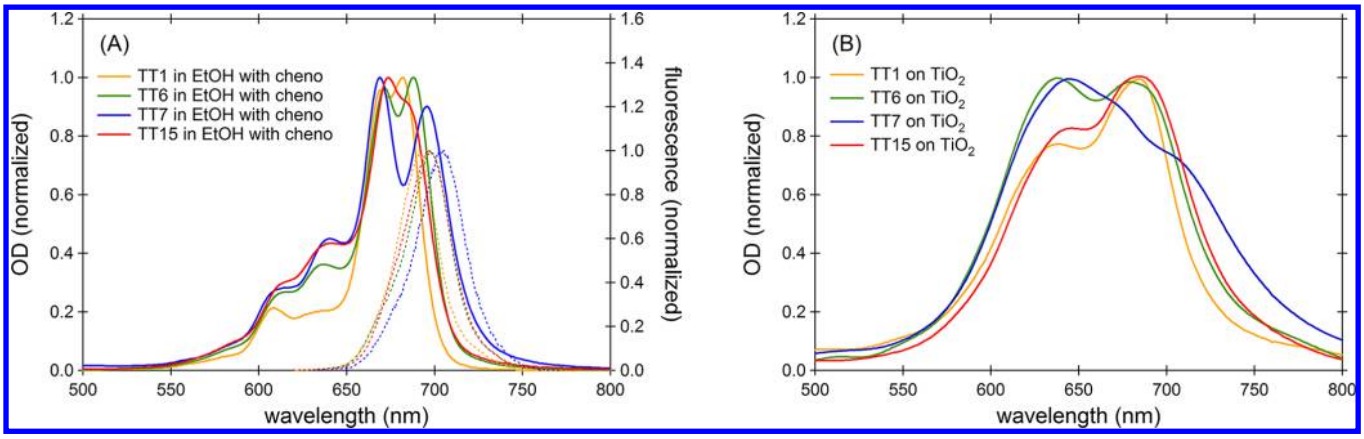

Figure 1. Absorption (solid lines) and fluorescence spectra (dotted lines) of TT1, TT6, TT7, and TT15 in EtOH containing chenodeoxycholic acid (A) and on nanocrystalline TiO_2 (B).

using a fused silica prism pair, yielding near transform-limited pump pulses at 670 nm with 30 nm fwhm bandwidth and 23 fs pulse duration. A fraction of the residual 775 nm fundamental light was focused onto a 2 mm sapphire window to create a white light continuum probe from 470 to 700 nm. The polarization between pump and probe was set at 54.7° to avoid anisotropy effects. The pump and probe beams were focused and spatially overlapped at the sample position. The pump pulse intensity was 5×10^{14} photons/cm^2 and was verified to be in the linear regime. The open-source software package Glotaran[37] was used for target analysis.

RESULTS AND DISCUSSION

Steady-State Absorption and Fluorescence Spectroscopy. Figure 1A shows the absorption and fluorescence spectra of TT1, TT6, TT7, and TT15 dissolved in a mixture of EtOH and chenodeoxycholic acid (cheno); the cosolvent is used to suppress aggregation. The Q-band ($S_0 \rightarrow S_1$) is split up due to the asymmetry of the molecule and shows maxima at 670 and 682 nm (TT1), 672 and 688 nm (TT6), 669 and 695 nm (TT7), and 674 and 687 nm (TT15). The absorption bands on the blue side are due to vibrational progression of the $S_0 \rightarrow S_1$ transition, possibly combined with the presence of minority $\pi-\pi$ stacked aggregates. Also included in Figure 1A are the fluorescence spectra obtained on excitation at 670 nm. The positions of the maxima (TT1: 691 nm, TT6: 697 nm, TT7: 704 nm, TT15: 696 nm) give a Stokes shift of 9 nm for all derivatives. The red-shift in absorption and fluorescence on going from TT1 to TT15, TT6, and TT7 is attributed to an increasing degree of delocalization on the bridge of the molecule.

Figure 1B shows the absorption spectra of TT1, TT6, TT7, and TT15 deposited onto nanocrystalline TiO_2. Obviously, the spectra are inhomogeneously broadened as compared to the solution spectra. In particular, the spectra of TT6 and TT7 show the presence of aggregates absorbing around 640 nm. Transient absorption measurements have been recorded on excitation at 670 nm to predominantly monitor the EI and BET dynamics originating from monomers and to suppress the contribution of aggregates. The fluorescence of all zinc phthalocyanine derivatives deposited onto TiO_2 has been observed to be heavily quenched (data not shown).

Transient Absorption Spectroscopy: TT1 in Solution. Figure 2 shows the transient absorption spectra of TT1 dissolved in a mixture of EtOH and cheno at time delays

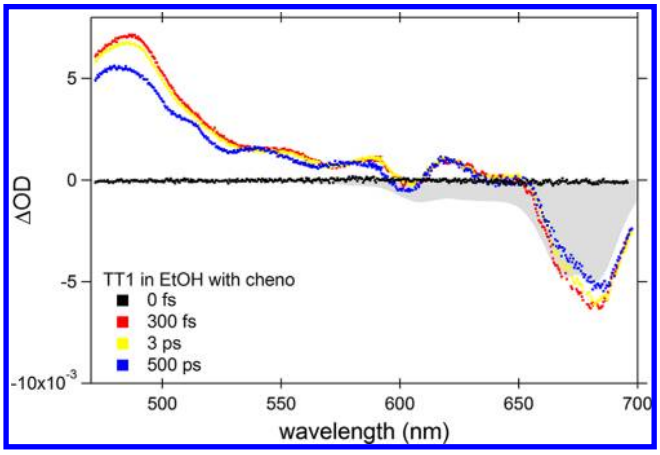

Figure 2. Transient spectra of TT1 in EtOH with cheno at various delays, recorded using an excitation wavelength centered at 670 nm. The gray area presents the inverted absorption spectrum (scaled).

ranging from 0 fs to 500 ps, recorded on excitation at 670 nm. Also included is the inverted absorption spectrum (gray area). A ground state bleach (GSB) in the range of 570−700 nm is formed instantaneously upon excitation. From comparison of the GSB signal and the inverted absorption spectrum, it is clear that predominantly monomers are excited and the contribution from aggregates (absorbing around 640 nm) is small. The broad excited state absorption (ESA) signal covers a wavelength range of 470 to 650 nm and is partially overlapping with the GSB. In addition, a stimulated emission (SE) signal around 690 nm is present. Spectra at the early time scales are similar; clearly no excited state decay occurs. The spectral shift at sub-ns time scale is due to intersystem crossing, as discussed in detail in our earlier work.[34,38]

Transient Absorption Spectroscopy: TT1 on TiO_2. Figure 3A shows the transient absorption spectra of TT1 on TiO_2 at time delays ranging from 0 fs to 500 ps, recorded on excitation at 670 nm. A GSB in the range of 550 to 700 nm is formed instantaneously upon excitation, as well as a broad ESA on the blue side of the spectrum and a SE signal in the range of 670 to 700 nm. The ESA clearly decays much faster than for TT1 in solution (Figure 2), which is due to EI into the TiO_2. The dynamics are independent of the excitation wavelength (Figure 4, Supporting Information), showing that vibrational relaxation is likely to occur within ~100 fs, as is also reported in the literature.[32,35] The contribution of the SE signal clearly

dx.doi.org/10.1021/jp410080a | J. Phys. Chem. C 2013, 117, 25397−25404

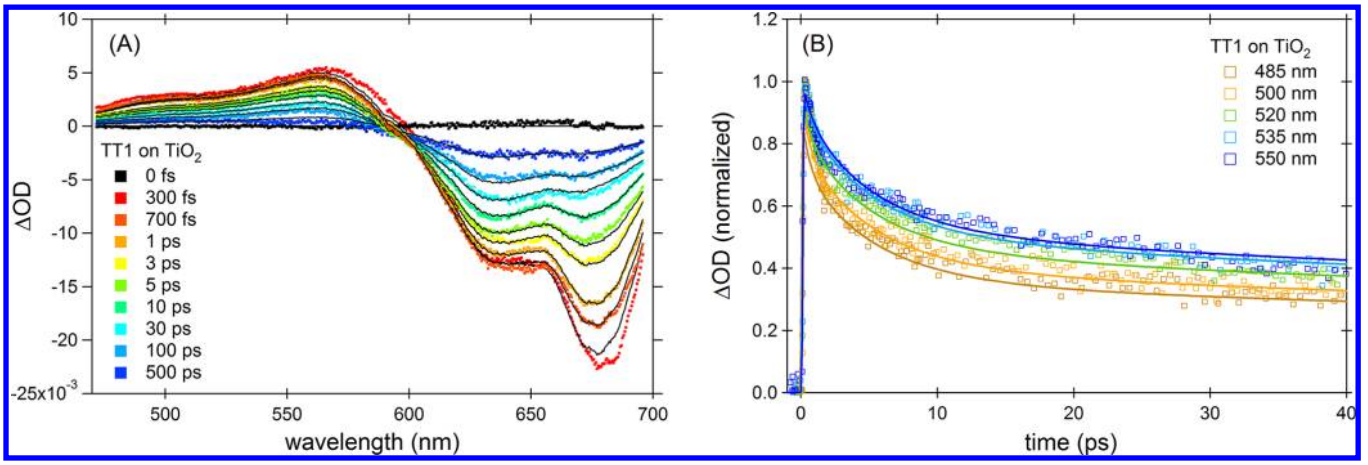

Figure 3. Transient absorption spectra and fits of TT1 on TiO_2 at various delays (A) and kinetic traces and fits at selected wavelengths (B).

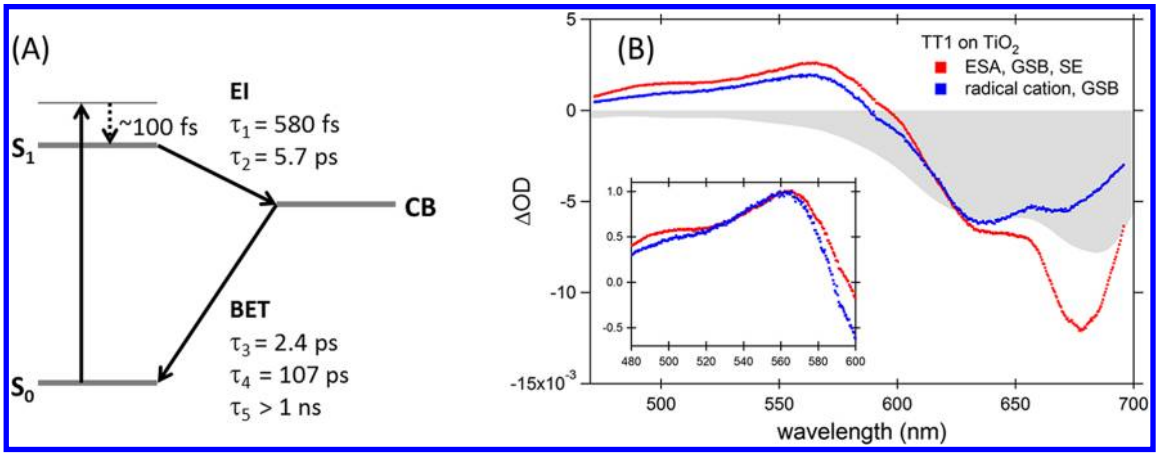

Figure 4. Qualitative energy level diagram for TT1 on TiO_2, showing the electron transfer pathways and the lifetimes obtained from (A) target analysis and (B) resolved species-associated spectra (SAS). The gray area presents the inverted absorption spectrum (scaled) and the inset shows a zoom-in of the normalized SAS.

decreases on going from 300 to 700 fs and has almost disappeared after 5 ps, showing that EI from TT1 into the TiO_2 predominantly occurs within the first 5 ps after excitation. The charge separated state formed is resembled by the absorption of the zinc phthalocyanine radical cation absorbing around 525 nm,[7] combined with a GSB signal. Figure 3B illustrates that moving from a probe wavelength of 485 to 550 nm leads to a slower decay. This shows that the TT1 radical cation has a red-shifted absorption as compared to the ESA signal. The absorption by the radical cation and the GSB signal simultaneously decrease at time scales ranging from the ps to the ns domain, showing that BET occurs over a broad time window.

Single wavelength analysis at selected wavelengths has been performed to determine the order of magnitude of lifetimes. The signal at 695 nm is largely due to SE (Figure 5, Supporting Information) and contains in addition a GSB contribution. The early time scale can be described by a biexponential decay with time scales of 0.7 and 8.8 ps, showing that (at least) two time constants are needed to describe the EI process. The existence of a third EI component within the instrumental response time cannot be excluded. A signature of BET involves the GSB recovery. The relative contribution of GSB to SE increases on moving from 695 to 630 nm (Figure 5, Supporting Information). The signal at 630 nm can be described by a triexponential decay function with time scales of 2.4 ps, 37 ps, and 0.75 ns.

Photophysical Modeling. The EI and BET dynamics have been quantified by spectrotemporal fitting to account for overlapping signals at one particular wavelength.[36] Figure 4A shows the photophysical model used for target analysis, performed using the software package Glotaran.[37] Intersystem crossing and internal conversion to the ground state occur on a ns time scale[38] and are therefore not included in the model. The absence of any excitation wavelength dependence (Figure 4, Supporting Information) shows that vibrational relaxation occurs on an ultrashort time scale (~100 fs), that is, prior to EI. As a first step, the rate constants τ_2, τ_4, and τ_5 have been determined while keeping τ_1 and τ_3 fixed at the values obtained from single wavelength analysis. Second, τ_1 has been optimized while keeping the values of all other parameters constant. Finally, τ_3 has been optimized while fixing all the rate constants at their optimized values. Table 1 presents the obtained lifetimes and amplitudes. Cross sections of the fit are included in Figure 3A,B. The data at nearly all times are well described by the fit, except at very early times, which may be due to an ultrafast (100−200 fs) EI process. The species-associated spectra (SAS) of TT1 on TiO_2 are shown in Figure 4B. The gray area presents the inverted absorption spectrum (scaled) and the inset shows a zoom-in of the normalized SAS. The SAS

dx.doi.org/10.1021/jp410080a | J. Phys. Chem. C 2013, 117, 25397−25404

Table 1. Lifetimes and Amplitudes (A) for Electron Injection (EI) and Back Electron Transfer (BET) Obtained from Target Analysis (Estimated Relative Error < 15%)

	EI		BET		
dye	τ_1 (ps) [A (%)]	τ_2 (ps) [A (%)]	τ_3 (ps) [A (%)]	τ_4 (ps) [A (%)]	τ_5 (ns) [A (%)]
TT7	0.7 [45]	22 [55]	2.1 [17]	88 [36]	0.7 [49]
TT6	0.7 [47]	16 [53]	1.9 [15]	113 [38]	>1.0 [47]
TT1	0.6 [46]	5.7 [54]	2.4 [17]	107 [39]	>1.0 [44]
TT15	0.6 [46]	5.8 [54]	3.0 [17]	112 [38]	>1.0 [45]

before EI (red) equals the spectrum at very early times, which consists of ESA, GSB, and SE signals. The SAS resembling the charge separated state (blue) is similar to the transient absorption spectrum at late times, at which EI is by far finalized, implying that the transient absorption spectrum contains contributions from the zinc phthalocyanine radical cation and the GSB signal only. Around 660−700 nm the SAS is less negative than expected on basis of the inverted absorption spectrum due to absorption by the radical cation in this region.[39,40]

Impact of the Anchoring Ligand. A fingerprint of the EI dynamics involves the decay of the ESA and SE signals. Figure 5A shows the kinetic traces at 500 nm for all four derivatives, at which wavelength the contribution of the ESA is relatively strong as compared to the absorption by the radical cation (see also the inset of Figure 4B). Clearly, the decay at 500 nm occurs the fastest for TT15 on TiO_2 and the slowest for TT7 on TiO_2, while TT1 and TT6 show intermediate behavior. The kinetic traces at 695 nm presented in Figure 5B are dominated by SE (see Figure 5, Supporting Information) and show a similar trend.

Target analysis should shed light on the quantitative differences in EI lifetimes. The full data sets of the other derivatives have been analyzed using a similar approach as described above for TT1 on TiO_2. The transient absorption spectra, fits, and SAS are presented in Figures 6−8 of the Supporting Information. For all derivatives the SAS before EI are equal to the transient spectra at very early times, while the SAS after EI and before BET are similar to the transient spectra at late times. The obtained lifetimes and amplitudes are presented in Table 1. Cross sections of the resulting fits are included in Figure 5A,B and show that the fits describe the data well. The fastest EI process (τ_1) occurs on a time scale of ∼700 fs for all four derivatives. The slower EI process (τ_2) occurs on similar fast time scales for TT1 (5.7 ps) and TT15 (5.8 ps) and is significantly slower for TT6 (16 ps) and TT7 (22 ps).

One possible explanation for the presence of two EI components is the two-state relaxation model, with a fast component originating from the nonthermalized state and a slower component due to the relaxed excited state.[18,20] However, our observation of excitation wavelength independent kinetics (Figure 4, Supporting Information) shows that this is unlikely for the zinc phthalocyanines studied, and vibrational relaxation occurs prior to EI. Another aspect to consider are crystal facets, which is likely to vary over the surface of the TiO_2 nanoparticle, affecting the binding mode and electronic coupling between the anchoring ligand and the TiO_2.[41] The slow EI process may also be related to aggregates. Injection by aggregates is known to be slow,[21,42] but indirect EI mediated by ps energy transfer toward a monomer[19,22] followed by ∼700 fs EI may be possible. Another explanation for the biexponential decay involves the simultaneous presence of two modes of monomer adsorption onto the TiO_2,[43,44] one facilitating the ∼700 fs EI independent of the anchoring ligand, and the second one leading to slower and ligand dependent EI. The comparable values for τ_1 for all derivatives suggests that this EI process does not occur via the anchoring ligand, but instead directly from the zinc phthalocyanine core toward the TiO_2, possibly via a through-space mechanism.[43] The second component can be attributed to a through-bond EI. Increasing the length of the spacer in between the anchoring ligand and the molecule (TT1 → TT6) slows down EI. Equipping the anchoring ligand with a CN group (TT6 → TT7) slows down EI even further and may be explained by the CN group acting as an electron trap. The negative effect of increasing the length of the spacer is compensated by introducing a second carboxylic acid group (TT6 → TT15). Both carboxylic acid groups are likely to be involved in bonding with the TiO_2,[41] increasing the electronic coupling and resulting in faster EI.

The signal at 630 nm largely consists of GSB and is therefore a good monitor for BET (Figure 5, Supporting Information). Figure 6 shows the kinetic traces at 630 nm for all four derivatives, including the fits resulting from target analysis. The obtained lifetimes for BET (τ_3, τ_4, τ_5) and amplitudes are

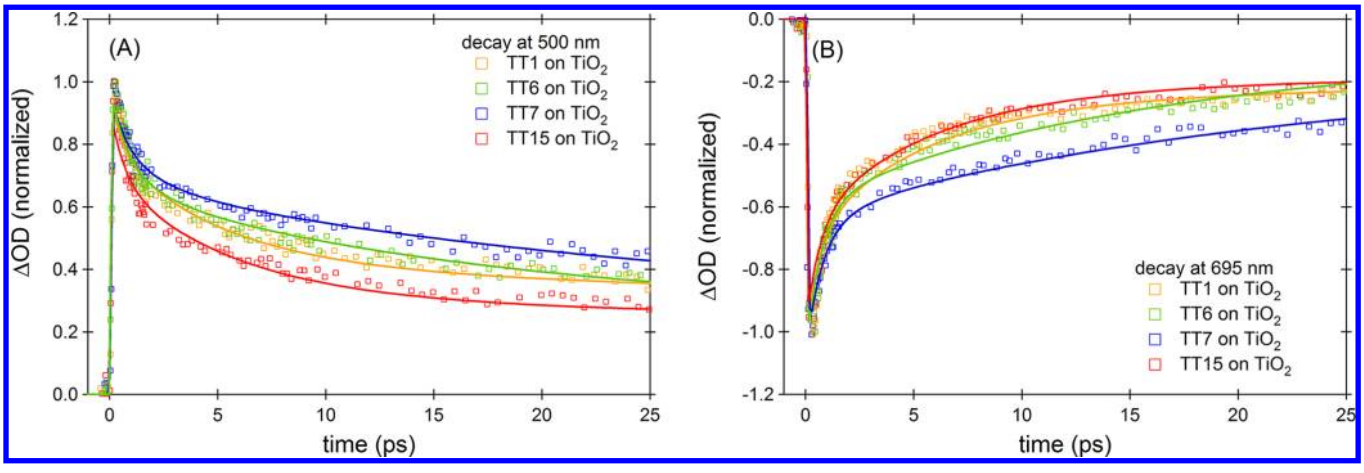

Figure 5. Kinetic traces at 500 nm showing the ESA decay (A) and at 695 nm resembling SE (B). The fits obtained using the model shown in Figure 2A and parameters presented in Table 1 are included.

dx.doi.org/10.1021/jp410080a | J. Phys. Chem. C 2013, 117, 25397−25404

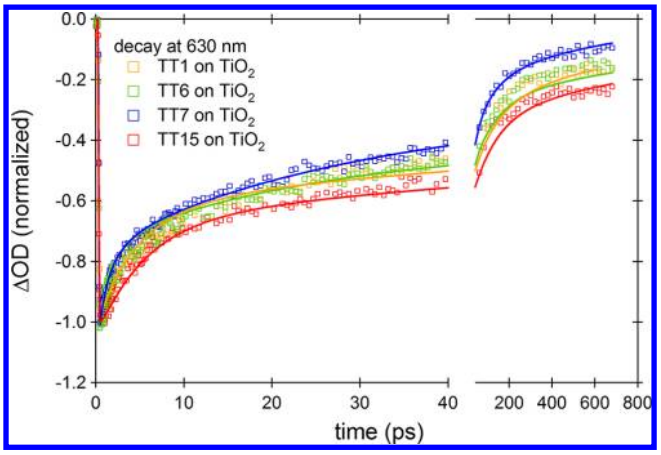

Figure 6. Kinetic traces at 630 nm resembling the GSB recovery. The fits obtained using the model shown in Figure 4A and parameters presented in Table 1 are included.

presented in Table 1. Obviously, BET occurs over a broad time window. Katoh and co-workers[44] report on a two-step charge separation process, with the first state being an electron−hole pair with still some Coulombic interaction, and the second state a completely dissociated electron−hole pair. TiO_2 nanoparticles are known to contain deep traps likely predominantly present at the surface[45−47] and shallow traps within the bulk.[48] The fast BET process can be attributed to recombination of electrons in deep surface trap with zinc phthalocyanine radical cations. Electrons may also escape from the deep surface traps and move into the bulk via a multiple trapping random walk process.[49] These electrons may eventually recombine with the zinc phthalocyanine radical cation, accounting for the slower BET processes. Also the occurrence of various TiO_2 crystal facets may play a role. It is obvious that TT15 shows the slowest recombination. The fastest BET step occurs significantly slower for TT15 than for the other derivatives, facilitating electrons to diffuse away from the interface. This could be due to a different bonding of monocarboxylic acids (TT1, TT6, and TT7) and dicarboxylic acids (TT15) with the TiO_2.[41] The dicarboxylic acid may also lead to a narrower distribution in molecular orientations. The inferior performance of TT7 as compared to TT1 and TT6 is likely due to the CN group, promoting BET.

CONCLUSIONS

We have performed a systematic study on the impact of the anchoring ligand of zinc phthalocyanine derivatives on the EI and BET dynamics by using femtosecond transient absorption spectroscopy. Kinetics are observed to be multiexponential with time scales ranging from sub-ps to ns. The best performing zinc phthalocyanine derivative, which is equipped with a dicarboxylic acid anchoring ligand (TT15, DSSC efficiency of 3.96%), shows the fastest overall EI. The EI process occurs via an ultrafast component (~700 fs for all derivatives) and a slower component (5.8 ps for TT15). The ps component is significantly slower for the other derivatives studied, up to 22 ps, for the derivative equipped with a CN group at the spacer in between the zinc phthalocyanine core and the anchoring carboxylic acid (TT7, DSSC efficiency of 2.55%). The observation that the ultrafast EI component is similar for all derivatives suggests that this EI process does not occur via the anchoring ligand but likely via a through-space mechanism instead. The ps EI process is most efficient in case the carboxylic acid is directly attached to the molecular core (TT1, DSSC efficiency of 3.56%) and becomes slower upon introducing a spacer (TT6) and a CN group (TT7). The effect of the spacer is compensated by introducing a second carboxylic acid anchoring group (TT15). Also, BET occurs via several components and is fastest for TT7 and slowest for TT15. The fastest recombination for TT7 is attributed to the CN acting as an electron trap. The higher efficiency of TT15 is likely due to the dicarboxylic acid binding mode promoting localized electrons to diffuse away rather than to recombine with the zinc phthalocyanine radical cation.

In conclusion, we have shown that modification of the anchoring ligand of zinc phthalocyanines is a powerful tool to manipulate both the EI and BET dynamics. A next step involves suppressing the slower EI in favor of the ~700 fs EI process. Mechanistic studies on whether the fast component is indeed due to a though-space transfer, and the slow component due to a through-bond mechanism would be highly valuable. Increasing the rigidity of the anchoring ligand, for example, by introducing triple bonds, may reduce the inhomogeneity in the molecular orientation. Also, the introduction of more carboxylic acid groups or a dicarboxylic acid group directly attached to the zinc phthalocyanine core, favoring only one molecular orientation, should be considered.

ASSOCIATED CONTENT

Supporting Information

Experimental methods, steady-state absorption and fluorescence spectra, and additional transient absorption data. This material is available free of charge via the Internet at http://pubs.acs.org.

AUTHOR INFORMATION

Corresponding Author

*E-mail: j.m.huijser@utwente.nl.

Notes

The authors declare no competing financial interest.

ACKNOWLEDGMENTS

Rick Elbersen of the Molecular Nanofabrication group, University of Twente, The Netherlands, is acknowledged for the Dektak measurement, and Joris Snellenburg of the Department of Physics and Astronomy, Vrije Universiteit Amsterdam, The Netherlands, for discussions regarding Glotaran. Financial support is acknowledged from the Nederlandse Organisatie voor Wetenschappelijk Onderzoek (NWO) and the Spanish MICINN (CTQ2011-24187/BQU, CTQ2011-23410/BQU and CONSOLIDER INGENIO 2010, CSD2007-00010 on Molecular Nanoscience) and the Comunidad de Madrid (MADRISOLAR-2, S2009/PPQ/1533).

REFERENCES

(1) Oregan, B.; Gratzel, M. A low-cost, high-efficiency solar cell based on dye-sensitized colloidal TiO_2 films. *Nature* **1991**, *353*, 737−740.

(2) Peter, L. M. The Gratzel cell: Where next? *J. Phys. Chem. Lett.* **2011**, *2*, 1861−1867.

(3) Yoneda, E.; Nazeeruddin, M. K.; Gratzel, M. Cyclometalated ruthenium dyes for DSSC. *J. Photopolym. Sci. Technol.* **2012**, *25*, 175−181.

(4) Nazeeruddin, M. K.; Humphry-Baker, R.; Gratzel, M.; Wohrle, D.; Schnurpfeil, G.; Schneider, G.; Hirth, A.; Trombach, N. Efficient near-IR sensitization of nanocrystalline TiO_2 films by zinc and

aluminum phthalocyanines. *J. Porphyrins Phthalocyanines* **1999**, *3*, 230−237.
(5) He, J. J.; Benko, G.; Korodi, F.; Polivka, T.; Lomoth, R.; Akermark, B.; Sun, L. C.; Hagfeldt, A.; Sundstrom, V. Modified phthalocyanines for efficient near-IR sensitization of nanostructured TiO_2 electrode. *J. Am. Chem. Soc.* **2002**, *124*, 4922−4932.
(6) Reddy, P. Y.; Giribabu, L.; Lyness, C.; Snaith, H. J.; Vijaykumar, C.; Chandrasekharam, M.; Lakshmikantam, M.; Yum, J. H.; Kalyanasundaram, K.; Gratzel, M.; Nazeeruddin, M. K. Efficient sensitization of nanocrystalline TiO_2 films by a near-IR-absorbing unsymmetrical zinc phthalocyanine. *Angew. Chem., Int. Ed.* **2007**, *46*, 373−376.
(7) Cid, J. J.; Garcia-Iglesias, M.; Yum, J. H.; Forneli, A.; Albero, J.; Martinez-Ferrero, E.; Vazquez, P.; Gratzel, M.; Nazeeruddin, M. K.; Palomares, E.; Torres, T. Structure-function relationships in unsymmetrical zinc phthalocyanines for dye-sensitized solar cells. *Chem.—Eur. J.* **2009**, *15*, 5130−5137.
(8) Ragoussi, M. E.; Cid, J. J.; Yum, J. H.; de la Torre, G.; Di Censo, D.; Gratzel, M.; Nazeeruddin, M. K.; Torres, T. Carboxyethynyl anchoring ligands: A means to improving the efficiency of phthalocyanine-sensitized solar cells. *Angew. Chem., Int. Ed.* **2012**, *51*, 4375−4378.
(9) Mori, S.; Nagata, M.; Nakahata, Y.; Yasuta, K.; Goto, R.; Kimura, M.; Taya, M. Enhancement of incident photon-to-current conversion efficiency for phthalocyanine-sensitized solar cells by 3D molecular structuralization. *J. Am. Chem. Soc.* **2010**, *132*, 4054−4055.
(10) Cid, J. J.; Yum, J. H.; Jang, S. R.; Nazeeruddin, M. K.; Ferrero, E. M.; Palomares, E.; Ko, J.; Gratzel, M.; Torres, T. Molecular cosensitization for efficient panchromatic dye-sensitized solar cells. *Angew. Chem., Int. Ed.* **2007**, *46*, 8358−8362.
(11) Martinez-Diaz, M. V.; de la Torre, G.; Torres, T. Lighting porphyrins and phthalocyanines for molecular photovoltaics. *Chem. Commun.* **2010**, *46*, 7090−7108.
(12) Garcia-Iglesias, M.; Yum, J. H.; Humphry-Baker, R.; Zakeeruddin, S. M.; Pechy, P.; Vazquez, P.; Palomares, E.; Gratzel, M.; Nazeeruddin, M. K.; Torres, T. Effect of anchoring groups in zinc phthalocyanine on the dye-sensitized solar cell performance and stability. *Chem. Sci.* **2011**, *2*, 1145−1150.
(13) Kimura, M.; Nomoto, H.; Masaki, N.; Mori, S. Dye molecules for simple co-sensitization process: Fabrication of mixed-dye-sensitized solar cells. *Angew. Chem., Int. Ed.* **2012**, *51*, 4371−4374.
(14) Kimura, M.; Nomoto, H.; Suzuki, H.; Ikeuchi, T.; Matsuzaki, H.; Murakami, T. N.; Furube, A.; Masaki, N.; Griffith, M. J.; Mori, S. Molecular design rule of phthalocyanine dyes for highly efficient near-IR performance in dye-sensitized solar cells. *Chem.—Eur. J.* **2013**, *19*, 7496−7502.
(15) Galoppini, E. Linkers for anchoring sensitizers to semiconductor nanoparticles. *Coord. Chem. Rev.* **2004**, *248*, 1283−1297.
(16) Sodeyama, K.; Sumita, M.; O'Rourke, C.; Terranova, U.; Isam, A.; Han, L. Y.; Bowler, D. R.; Tateyama, Y. Protonated carboxyl anchor for stable adsorption of Ru N749 dye (Black Dye) on a TiO_2 anatase (101) surface. *J. Phys. Chem. Lett.* **2012**, *3*, 472−477.
(17) Marcus, R. A. On theory of electron-transfer reactions 0.6. Unified treatment for homogeneous and electrode reactions. *J. Chem. Phys.* **1965**, *43*, 679−701.
(18) Anderson, N. A.; Lian, T. Q. Ultrafast electron transfer at the molecule-semiconductor nanoparticle interface. *Annu. Rev. Phys. Chem.* **2005**, *56*, 491−519.
(19) Luo, L. Y.; Lo, C. F.; Lin, C. Y.; Chang, I. J.; Diau, E. W. G. Femtosecond fluorescence dynamics of porphyrin in solution and solid films: The effects of aggregation and interfacial electron transfer between porphyrin and TiO_2. *J. Phys. Chem. B* **2006**, *110*, 410−419.
(20) Pijpers, J. J. H.; Ulbricht, R.; Derossi, S.; Reek, J. N. H.; Bonn, M. Picosecond electron injection dynamics in dye-sensitized oxides in the presence of electrolyte. *J. Phys. Chem. C* **2011**, *115*, 2578−2584.
(21) Teuscher, J.; Decoppet, J. D.; Punzi, A.; Zakeeruddin, S. M.; Moser, J. E.; Gratzel, M. Photoinduced interfacial electron injection dynamics in dye-sensitized solar cells under photovoltaic operating conditions. *J. Phys. Chem. Lett.* **2012**, *3*, 3786−3790.
(22) Li, Y.; Lu, P. F.; Yan, X. Z.; Jin, L.; Peng, Z. H. Non-aggregated hyperbranched phthalocyanines: single molecular nanostructures for efficient semi-opaque photovoltaics. *RSC Adv.* **2013**, *3*, 545−558.
(23) Ramakrishna, G.; Jose, D. A.; Kumar, D. K.; Das, A.; Palit, D. K.; Ghosh, H. N. Strongly coupled ruthenium-polypyridyl complexes for efficient electron injection in dye-sensitized semiconductor nanoparticles. *J. Phys. Chem. B* **2005**, *109*, 15445−15453.
(24) Ramakrishna, G.; Verma, S.; Jose, D. A.; Kumar, D. K.; Das, A.; Palit, D. K.; Ghosh, H. N. Interfacial electron transfer between the photoexcited porphyrin molecule and TiO_2 nanoparticles: Effect of catecholate binding. *J. Phys. Chem. B* **2006**, *110*, 9012−9021.
(25) Verma, S.; Ghosh, H. N. Exciton Energy and Charge Transfer in Porphyrin Aggregate/Semiconductor TiO_2 Composites. *J. Phys. Chem. Lett.* **2012**, *3*, 1877−1884.
(26) Huijser, A.; Savenije, T. J.; Siebbeles, L. D. A. Effect of the structure of substituents on charge separation in meso-tetraphenylporphyrin/TiO_2 bilayers. *Thin Solid Films* **2006**, *511*, 208−213.
(27) Huijser, A.; Savenije, T. J.; Kroeze, J. E.; Siebbeles, L. D. A. Exciton diffusion and interfacial charge separation in meso-tetraphenylporphyrin/TiO_2 bilayers: Effect of ethyl substituents. *J. Phys. Chem. B* **2005**, *109*, 20166−20173.
(28) Asbury, J. B.; Hao, E.; Wang, Y. Q.; Ghosh, H. N.; Lian, T. Q. Ultrafast electron transfer dynamics from molecular adsorbates to semiconductor nanocrystalline thin films. *J. Phys. Chem. B* **2001**, *105*, 4545−4557.
(29) Lin, C. Y.; Lo, C. F.; Luo, L.; Lu, H. P.; Hung, C. S.; Diau, E. W. G. Design and characterization of novel porphyrins with oligo-(phenylethylnyl) links of varied length for dye-sensitized solar cells: Synthesis and optical, electrochemical, and photovoltaic investigation. *J. Phys. Chem. C* **2009**, *113*, 755−764.
(30) Chang, C. W.; Luo, L. Y.; Chou, C. K.; Lo, C. F.; Lin, C. Y.; Hung, C. S.; Lee, Y. P.; Diau, E. W. G. Femtosecond transient absorption of zinc porphyrins with oligo(phenylethylnyl) linkers in solution and on TiO_2 films. *J. Phys. Chem. C* **2009**, *113*, 11524−11531.
(31) Wiberg, J.; Marinado, T.; Hagberg, D. P.; Sun, L. C.; Hagfeldt, A.; Albinsson, B. Effect of anchoring group on electron injection and recombination dynamics in organic dye-sensitized solar cells. *J. Phys. Chem. C* **2009**, *113*, 3881−3886.
(32) Ino, D.; Watanabe, K.; Takagi, N.; Matsumoto, Y. Electron transfer dynamics from organic adsorbate to a semiconductor surface: Zinc phthalocyanine on TiO_2(110). *J. Phys. Chem. B* **2005**, *109*, 8018−18024.
(33) Garcia-Iglesias, M.; Cid, J. J.; Yum, J. H.; Forneli, A.; Vazquez, P.; Nazeeruddin, M. K.; Palomares, E.; Gratzel, M.; Torres, T. Increasing the efficiency of zinc-phthalocyanine based solar cells through modification of the anchoring ligand. *Energy Environ. Sci.* **2011**, *4*, 189−194.
(34) Sharma, D.; Huijser, A.; Savolainen, J.; Steen, G.; Herek, J. L. Active and passive control of zinc phthalocyanine photodynamics. *Faraday Discuss.* **2013**, *163*, 433−445.
(35) Berera, R.; Herrero, C.; van Stokkum, I. H. M.; Vengris, M.; Kodis, G.; Palacios, R. E.; van Amerongen, H.; van Grondelle, R.; Gust, D.; Moore, T. A.; Moore, A. L.; Kennis, J. T. M. A simple artificial light-harvesting dyad as a model for excess energy dissipation in oxygenic photosynthesis. *Proc. Natl. Acad. Sci. U.S.A.* **2006**, *103*, 5343−5348.
(36) van Stokkum, I. H. M.; Larsen, D. S.; van Grondelle, R. Global and target analysis of time-resolved spectra. *Biochim. Biophys. Acta, Bioenerg.* **2004**, *1657*, 82−104.
(37) Snellenburg, J. J.; Laptenok, S. P.; Seger, R.; Mullen, K. M.; van Stokkum, I. H. M. Glotaran: A Java-based graphical user interface for the R package TIMP. *J. Stat. Software* **2012**, *49*, 1−22.
(38) Savolainen, J.; van der Linden, D.; Dijkhuizen, N.; Herek, J. L. Characterizing the functional dynamics of zinc phthalocyanine from femtoseconds to nanoseconds. *J. Photochem. Photobiol. A* **2008**, *196*, 99−105.
(39) Charlesworth, P.; Truscott, T. G.; Brooks, R. C.; Wilson, B. C. The photophysical properties of a ruthenium-substitited phthalocyanine. *J. Photochem. Photobiol. B* **1994**, *26*, 277−282.

(40) Jimenez, A. J.; Grimm, B.; Gunderson, V. L.; Vagnini, M. T.; Calderon, S. K.; Rodriguez-Morgade, M. S.; Wasielewski, M. R.; Guldi, D. M.; Torres, T. Synthesis, characterization, and photoinduced energy and electron transfer in a supramolecular tetrakis (ruthenium(II) phthalocyanine) perylenediimide pentad. *Chem.—Eur. J.* **2011**, *17*, 5024−5032.
(41) Thomas, A. G.; Syres, K. L. Adsorption of organic molecules on rutile TiO_2 and anatase TiO_2 single crystal surfaces. *Chem. Soc. Rev.* **2012**, *41*, 4207−4217.
(42) Wang, X. C.; Yu, J. C. Nonaggregated zinc phthalocyanine in mesoporous nanocrystalline TiO_2 thin films. *Macromol. Rapid Commun.* **2004**, *25*, 1414−1418.
(43) Imahori, H.; Kang, S.; Hayashi, H.; Haruta, M.; Kurata, H.; Isoda, S.; Canton, S. E.; Infahsaeng, Y.; Kathiravan, A.; Pascher, T.; Chabera, P.; Yartsev, A. P.; Sundstrom, V. Photoinduced charge carrier dynamics of Zn-porphyrin-TiO_2 electrodes: The key role of charge recombination for solar cell performance. *J. Phys. Chem. A* **2011**, *115*, 3679−3690.
(44) Katoh, R.; Furube, A.; Fuke, N.; Fukui, A.; Koide, N. Ultrafast relaxation as a possible limiting factor of electron injection efficiency in black dye sensitized nanocrystalline TiO_2 Films. *J. Phys. Chem. C* **2012**, *116*, 22301−22306.
(45) Boschloo, G.; Hagfeldt, A. Activation energy of electron transport in dye-sensitized TiO_2 solar cells. *J. Phys. Chem. B* **2005**, *109*, 12093−12098.
(46) Kopidakis, N.; Benkstein, K. D.; van de Lagemaat, J.; Frank, A. J.; Yuan, Q.; Schiff, E. A. Temperature dependence of the electron diffusion coefficient in electrolyte-filled TiO_2 nanoparticle films: Evidence against multiple trapping in exponential conduction-band tails. *Phys. Rev. B* **2006**, *73*, 045326.
(47) Savenije, T. J.; Huijser, A.; Vermeulen, M. J. W.; Katoh, R. Charge carrier dynamics in TiO_2 nanoparticles at various temperatures. *Chem. Phys. Lett.* **2008**, *461*, 93−96.
(48) Di Valentin, C.; Selloni, A. Bulk and Surface Polarons in Photoexcited Anatase TiO_2. *J. Phys. Chem. Lett.* **2011**, *2*, 2223−2228.
(49) Nelson, J.; Haque, S. A.; Klug, D. R.; Durrant, J. R. Trap-limited recombination in dye-sensitized nanocrystalline metal oxide electrodes. *Phys. Rev. B* **2011**, *63*, 205321.